

# SAE 4620 Quenched Core Steel Iteration #53

Fatigue Behavior, Monotonic Properties  
and  
Microstructural Data

Prepared by:

F. Yin  
and  
A. Fatemi

Department of Mechanical, Industrial and  
Manufacturing Engineering  
The University of Toledo  
Toledo, Ohio 43606

Prepared for:  
The AISI Bar Steel Applications Group

March 2002



American Iron and Steel Institute  
2000 Town Center, Suite 320  
Southfield, Michigan 48075  
tel: 248-945-4777  
fax: 248-352-1740  
[www.autosteel.org](http://www.autosteel.org)

# TABLE OF CONTENTS

<b>SUMMARY .....</b>	<b>1</b>
<b>I. EXPERIMENTAL PROGRAM .....</b>	<b>2</b>
1.1 MATERIAL AND SPECIMEN FABRICATION .....	2
<i>1.1.1 Material .....</i>	<i>2</i>
<i>1.1.2 Specimen .....</i>	<i>2</i>
1.2 TESTING EQUIPMENT .....	3
<i>1.2.1 Apparatus .....</i>	<i>3</i>
<i>1.2.2 Alignment .....</i>	<i>4</i>
1.3 TEST METHODS AND PROCEDURES .....	5
<i>1.3.1 Monotonic tension tests .....</i>	<i>5</i>
<i>1.3.2 Constant amplitude fatigue tests .....</i>	<i>6</i>
<b>II. EXPERIMENTAL RESULTS AND ANALYSIS .....</b>	<b>7</b>
2.1 MICROSTRUCTURAL DATA .....	7
2.2 MONOTONIC DEFORMATION BEHAVIOR .....	8
2.3 CYCLIC DEFORMATION BEHAVIOR .....	10
<i>2.3.1 Transient cyclic deformation .....</i>	<i>10</i>
<i>2.3.2 Steady-state cyclic deformation .....</i>	<i>10</i>
2.4 CONSTANT AMPLITUDE FATIGUE BEHAVIOR .....	12
<b>REFERENCES .....</b>	<b>27</b>
<b>APPENDIX .....</b>	<b>28</b>

## NOMENCLATURE

$A_o, A_f$	initial, final area	S	engineering stress
HB, HRB, HRC	Brinell, Rockwell B-Scale, Rockwell C-Scale hardness number	YS, UYS, LYS, YS'	monotonic yield, upper yield, lower yield, cyclic yield strength
b, c, n	fatigue strength, fatigue ductility, strain hardening exponent	YPE	yield point elongation
$D_o, D_f$	initial, final diameter	$S_u$	ultimate tensile strength
e	engineering strain	%EL	percent elongation
E, E'	monotonic, midlife cycle modulus of elasticity	%RA	percent reduction in area
K, K'	monotonic, cyclic strength coefficient	$\sigma, \sigma_f, \sigma_f'$	true stress, true fracture strength, fatigue strength coefficient
$L_o, L_f$	initial, final gage length	$\sigma_a, \sigma_m, \Delta\sigma$	stress amplitude, mean stress, stress range
$N_{50\%},$ $(N_f)_{10\%},$ $(N_f)_{50\%},$	number of cycles to midlife, 10% load drop, 50% load drop	$\epsilon_e, \epsilon_p, \epsilon$	true elastic, plastic, total strain
$2N_f$	reversals to failure	$\epsilon_f, \epsilon_f'$	true fracture ductility, fatigue ductility coefficient
$P_f, P_u$	fracture, ultimate load	$\epsilon_a, \epsilon_m, \Delta\epsilon$	strain amplitude, mean strain, strain range
R	neck radius; or strain ratio	$\Delta\epsilon_e, \Delta\epsilon_p$	elastic, plastic strain range

## UNIT CONVERSION TABLE

<u>Measure</u>	<u>SI Unit</u>	<u>US Unit</u>	<u>from SI to US</u>	<u>from US to SI</u>
Length	mm	in	1 mm = 0.03937 in	1 in = 25.4 mm
Area	mm <sup>2</sup>	in <sup>2</sup>	1 mm <sup>2</sup> = 0.00155 in <sup>2</sup>	1 in <sup>2</sup> = 645.16 mm <sup>2</sup>
Load	kN	klb	1kN = 0.2248 klb	1 klb = 4.448 kN
Stress	MPa	ksi	1 MPa = 0.14503 ksi	1 ksi = 6.895 MPa
Temperature	°C	°F	°C = (°F - 32)/1.8	°F = (°C * 1.8) + 32

<u>In SI Unit:</u>	1 kN = 10 <sup>3</sup> N	1 Pa = 1 N/m <sup>2</sup>	1 MPa = 10 <sup>6</sup> Pa = 1 N/mm <sup>2</sup>	1 Gpa = 10 <sup>9</sup> Pa
<u>In US Unit:</u>	1 klb = 10 <sup>3</sup> lb	1 psi = 1 lb/in <sup>2</sup>	1 ksi = 10 <sup>3</sup> psi	

## **SUMMARY**

The monotonic properties, and fatigue behavior data have been obtained for SAE 4620 Quenched Core steel. The material was provided by MacSteel Company. Two tensile tests were performed to acquire the desired monotonic properties. Eighteen strain-controlled fatigue tests were performed to obtain the strain-life and cyclic stress-strain curves and properties. The experimental procedure followed and results obtained are presented and discussed in this report.

# **I. EXPERIMENTAL PROGRAM**

## **1.1 Material and Specimen Fabrication**

### **1.1.1 Material**

The SAE 4620 Quenched Core steel was provided by MacSteel Company. This material was delivered to the University of Toledo in round bar form. The bars were approximately 1.875 inch in diameter. They were reduced to bars approximately 0.5 inch diameter by EDM, then heat treated prior to machining. In Table 1, the chemical composition supplied by AISI is shown.

### **1.1.2 Specimen**

In this study, identical round specimens were used for the monotonic and fatigue tests. The specimen configuration and dimensions are shown in Figure 1. This configuration deviates slightly from the specimens recommended by ASTM Standard E606 [1]. The recommended specimens have uniform or hourglass test sections. The specimen geometry shown in Figure 1 differs by using a large secondary radius throughout the test section.

All specimens were machined in the Mechanical, Industrial, and Manufacturing Engineering Machine Shop at the University of Toledo. The specimens were cut to the appropriate length, after that center-drilled in both ends and inserted into a CNC machine. Using the CNC machine, final turning was performed to achieve the tolerable dimensions specified on the specimen drawings.

A commercial round-specimen polishing machine was used to polish the specimen gage section. Four different grits of aluminum oxide lapping film were used: 30 $\mu$ , 15 $\mu$ , 9 $\mu$ , and 3 $\mu$ . The 3 $\mu$  grit was used as the final polish and polishing marks coincided with the specimens' longitudinal direction. The polished surfaces were carefully examined under magnification to ensure complete removal of machine marks within the test section.

## **1.2 Testing Equipment**

### **1.2.1 Apparatus**

An MTS closed-loop servo-controlled hydraulic axial load frame in conjunction with a Schenck-Pegasus digital servo-controller was used to conduct the tests. The calibration of this system was verified prior to beginning the test program. The load cell used had a capacity of 22 klb. Hydraulically operated grips using universal tapered collets were employed to secure the specimens' ends in series with the load cell.

Total strain was controlled for all tests using an extensometer rated as ASTM class B1 [2]. The calibration of the extensometer was verified using displacement apparatus containing a micrometer barrel in divisions of 0.0001 in. The extensometer had a gage length of 0.30 in and was capable of measuring strains up to 15 %.

In order to protect the specimens' surface from the knife-edges of the extensometer, ASTM Standard E606 recommends the use of transparent tape or epoxy to 'cushion' the attachment. For this study, it was found that application of transparent tape strips was difficult due to the radius within the test section. Therefore, epoxy was

considered to be the best protection. One disadvantage of epoxy is the variability of mixtures throughout the test program. As an alternative to epoxy, M-coat D offered a more consistent mixture. Therefore, the tests were performed using M-coat D.

All tests were conducted at room temperature and were monitored using a digital thermometer. In order to minimize temperature effects upon the extensometer and load cell calibrations, fluctuations were maintained within  $\pm 2$  °C ( $\pm 3.6$  °F) as required by ASTM Standard E606. Also, the relative humidity of the air was monitored using a precision hydrometer.

### **1.2.2 Alignment**

Significant effort was put forth to align the load train (load cell, grips, specimen, and actuator). Misalignment can result from both tilt and offset between the central lines of the load train components. According to ASTM Standard E606, the maximum bending strains should not exceed 5 % of the minimum axial strain range imposed during any test program. For this study, the minimum axial strain range was 0.0045 in/in. Therefore, the maximum allowable bending strain was 225 microstrain. ASTM Standard E1012, Type A, Method 1 was followed to verify specimen alignment [3]. For this procedure, two arrays of four strain gages per array were arranged at the upper and lower ends of the uniform gage section. For each array, gages were equally spaced around the circumference of a 0.5-in. uniform diameter bar. The maximum bending strain determined from the gaged specimen was less than 30 microstrain. This value was well within the allowable ASTM limit.



## **1.3 Test Methods and Procedures**

### **1.3.1 Monotonic tension tests**

All monotonic tests in this study were performed using test methods specified by ASTM Standard E8 [4]. Two specimens were used to obtain the monotonic properties. Due to the limitations of the extensometer, strain control was used only up to 14% strain. After this point, displacement control was used until fracture.

For the elastic and initial yield region (0% to 0.5% strain), a strain rate of 0.0025 in/in/min was chosen. This strain rate was three-quarters of the maximum allowable rate specified by ASTM Standard E8 for the initial yield region. After yielding (0.5% to 14% strain), the strain rate was increased by a factor of three (i.e., 0.0075 in/in/min). After the extensometer was removed, a displacement rate of 0.01275 in/min was used. This displacement rate provided approximately the same strain rate as that used prior to switching control modes.

After the tension tests were concluded, the broken specimens were carefully reassembled. The final gage lengths of the fractured specimens were measured with a Vernier caliper having divisions of 0.001 in. Using an optical comparator with 10X magnification and divisions of 0.001 in, the final diameter and the neck radius were measured. It should be noted that prior to the test, the initial minimum diameter was measured with this same instrument.

### **1.3.2 Constant amplitude fatigue tests**

All constant amplitude fatigue tests in this study were performed according to ASTM Standard E606. It is recommended by this standard that at least 10 specimens be used to generate the fatigue properties. For this study, 18 specimens at 6 different strain amplitudes ranging from 0.225% to 2% were utilized. LabVIEW by National Instrument was used to record the hysteresis loops.

There were two control modes used for these tests. Strain control was used in all tests, except the run-out tests. For the run-out tests (greater than  $5 \times 10^6$  cycles), strain control was used initially to determine the stabilized load. Then stress control was used for the remainder of the test. The reason for the change in control mode was due to limitations on the extensometer. For the strain control tests, the applied frequencies ranged from 0.20 Hz to 3.0 Hz in order to keep a strain rate about 0.02 in/in/sec. For the stress control tests, the frequency was increased to 30 Hz in order to shorten the overall test duration. All strain control tests were conducted using a triangular waveform.

## **II. EXPERIMENTAL RESULTS AND ANALYSIS**

### **2.1 Microstructural Data**

Photomicrographs of the microstructure were obtained using an optical microscope with a digital camera attachment. In Figure 2, the longitudinal direction is shown at 500X magnification. It can be seen from this photomicrograph that SAE 4620 Quenched Core steel had a ferrite/pearlite microstructure. In Figure 3, the inclusions/voids in L-T direction are shown at 100X magnification. For Figures 2 and 3, the rolling direction is horizontal to the page.

According to ASTM Standard E45, method A, the inclusion rating number for type A inclusion in L-T direction was found [6]. Brinell and Rockwell hardness tests were also performed. A summary of the microstructural data for SAE 4620 Quenched Core steel is provided in Table 2.

## 2.2 Monotonic Deformation Behavior

The properties determined from monotonic tests were the following: modulus of elasticity (E), yield strength (YS), upper yield strength (UYS), lower yield strength (LYS), yield point elongation (YPE), ultimate tensile strength ( $S_u$ ), percent elongation (%EL), percent reduction in area (%RA), true fracture strength ( $\sigma_f$ ), true fracture ductility ( $\epsilon_f$ ), strength coefficient (K), and strain hardening exponent (n).

True stress ( $\sigma$ ), true strain ( $\epsilon$ ), and true plastic strain ( $\epsilon_p$ ) were calculated from engineering stress (S) and engineering strain (e), according to the following relationships which are based on constant volume assumption:

$$\sigma = S(1 + e) \quad (1a)$$

$$\epsilon = \ln(1 + e) \quad (1b)$$

$$\epsilon_p = \epsilon - \epsilon_e = \epsilon - \frac{\sigma}{E} \quad (1c)$$

The true stress ( $\sigma$ ) - true strain ( $\epsilon$ ) plot is often represented by the Ramberg-Osgood equation:

$$\epsilon = \epsilon_e + \epsilon_p = \frac{\sigma}{E} + \left( \frac{\sigma}{K} \right)^{\frac{1}{n}} \quad (2)$$

The strength coefficient, K, and strain hardening exponent, n, are the intercept and slope of the best line fit to true stress ( $\sigma$ ) versus true plastic strain ( $\epsilon_p$ ) data in log-log scale:

$$\sigma = K \left( \epsilon_p \right)^n \quad (3)$$

In accordance with ASTM Standard E739 [7], when performing the least squares fit, the true plastic strain ( $\epsilon_p$ ) was the independent variable and the stress ( $\sigma$ ) was the dependent variable. These plots for the two tests conducted are shown in Figure 4. To generate the K and n values, the range of data used in this figure was chosen according to the definition of discontinuous yielding specified in ASTM Standard E646 [8]. Therefore, the valid data range occurred between the end of yield point extension and the strain at or prior to maximum load.

The true fracture strength,  $\sigma_f$ , was corrected for necking according to the Bridgman correction factor [9]:

$$\sigma_f = \frac{\frac{P_f}{A_f}}{\left(1 + \frac{4R}{D_f}\right) \ln\left(1 + \frac{D_f}{4R}\right)} \quad (4)$$

where  $P_f$  is the load at fracture,  $R$  is the neck radius, and  $D_f$  is the diameter at fracture.

The true fracture ductility,  $\epsilon_f$ , was calculated from the relationship based on constant volume:

$$\epsilon_f = \ln\left(\frac{A_o}{A_f}\right) = \ln\left(\frac{1}{1 - RA}\right) \quad (5)$$

where  $A_f$  is the cross-sectional area at fracture,  $A_o$  is the original cross-sectional area, and  $RA$  is the reduction in area.

A summary of the monotonic properties for SAE 4620 Quenched Core steel is provided in Table 2. The monotonic stress-strain curves are shown in Figure 5. As can be

seen from this figure, the two curves are close to each other. Refer to Table A.1 in the Appendix for a summary of the monotonic test results.

## **2.3 Cyclic Deformation Behavior**

### **2.3.1 Transient cyclic response**

Transient cyclic response describes the process of cyclic-induced change in deformation resistance of a material. Data obtained from constant amplitude strain-controlled fatigue tests were used to determine this response. Plots of stress amplitude variation versus applied number of cycles can indicate the degree of transient cyclic softening/hardening. Also, these plots show when cyclic stabilization occurs. A composite plot of the transient cyclic response for SAE 4620 Quenched Core steel is shown in Figure A.1 of the Appendix. The transient response was normalized on the rectangular plot in Figure A.1a, while a semi-log plot is shown in Figure A.1b. Even though multiple tests were conducted at each strain amplitude, data from one test at each strain amplitude tested are shown in these plots.

### **2.3.2 Steady-state cyclic deformation**

Another cyclic behavior of interest was the steady state or stable response. Data obtained from constant amplitude strain-controlled fatigue tests were also used to determine this response. The properties determined from the steady-state hysteresis loops were the following: cyclic modulus of elasticity ( $E'$ ), cyclic strength coefficient ( $K'$ ),

cyclic strain hardening exponent ( $n'$ ), and cyclic yield strength (YS'). Half-life (midlife) hysteresis loops and data were used to obtain the stable cyclic properties.

Similar to monotonic behavior, the cyclic true stress-strain behavior can be characterized by the Ramberg-Osgood type equation:

$$\frac{\Delta \varepsilon}{2} = \frac{\Delta \varepsilon_e}{2} + \frac{\Delta \varepsilon_p}{2} = \frac{\Delta \sigma}{2 E} + \left( \frac{\Delta \sigma}{2 K'} \right)^{\frac{1}{n'}} \quad (6)$$

It should be noted that in Equation 6 and the other equations that follow, E is the average modulus of elasticity that was calculated from the monotonic tests.

The cyclic strength coefficient,  $K'$ , and cyclic strain hardening exponent,  $n'$ , are the intercept and slope of the best line fit to true stress amplitude ( $\Delta\sigma/2$ ) versus true plastic strain amplitude ( $\Delta\varepsilon_p/2$ ) data in log-log scale:

$$\frac{\Delta \sigma}{2} = K' \left( \frac{\Delta \varepsilon_p}{2} \right)^{n'} \quad (7)$$

In accordance with ASTM Standard E739, when performing the least squares fit, the true plastic strain amplitude ( $\Delta\varepsilon_p/2$ ) was the independent variable and the stress amplitude ( $\Delta\sigma/2$ ) was the dependent variable. The true plastic strain amplitude was calculated by the following equation:

$$\frac{\Delta \varepsilon_p}{2} = \frac{\Delta \varepsilon}{2} - \frac{\Delta \sigma}{2 E} \quad (8)$$

This plot is shown in Figure 6. To generate the  $K'$  and  $n'$  values, the range of data used in the figure was chosen for  $[\Delta\varepsilon_p/2]_{\text{calculated}} \geq 0.00020$  in/in and  $N_f \leq 10^5$  cycles.

The cyclic stress - strain curve reflects the resistance of a material to cyclic deformation and can be vastly different from the monotonic stress - strain curve. The

cyclic stress - strain curve is shown in Figure 7. In Figure 8, superimposed plots of monotonic and cyclic curves are shown. As can be seen in Figure 8, SAE 4620 Carburized Case steel cyclically hardens before 2% strain. Figure A.2 in the Appendix shows a composite plot of the steady-state (midlife) hysteresis loops. Even though multiple tests were conducted at each strain amplitude, the stable loops from only one test at each strain amplitude are shown in this plot.

## 2.4 Constant Amplitude Fatigue Behavior

Constant amplitude strain-controlled fatigue tests were performed to determine the strain-life curve. The following equation relates the true strain amplitude to the fatigue life:

$$\frac{\Delta \varepsilon}{2} = \frac{\Delta \varepsilon_e}{2} + \frac{\Delta \varepsilon_p}{2} = \frac{\sigma_f'}{E} (2 N_f)^b + \varepsilon_f' (2 N_f)^c \quad (9)$$

where  $\sigma_f'$  is the fatigue strength coefficient,  $b$  is the fatigue strength exponent,  $\varepsilon_f'$  is the fatigue ductility coefficient,  $c$  is the fatigue ductility exponent,  $E$  is the monotonic modulus of elasticity, and  $2N_f$  is the number of reversals to failure (which was defined as a 50% tensile load drop, as recommended by ASTM Standard E606).

The fatigue strength coefficient,  $\sigma_f'$ , and fatigue strength exponent,  $b$ , are the intercept and slope of the best line fit to true stress amplitude ( $\Delta\sigma/2$ ) versus reversals to failure ( $2N_f$ ) data in log-log scale:

$$\frac{\Delta \sigma}{2} = \sigma_f' (2 N_f)^b \quad (10)$$



In accordance with ASTM Standard E739, when performing the least squares fit, the stress amplitude ( $\Delta\sigma/2$ ) was the independent variable and the reversals to failure ( $2N_f$ ) was the dependent variable. This plot is shown in Figure 9. To generate the  $\sigma_f'$  and  $b$  values, the range of data used in this figure was chosen for  $N_f \leq 10^5$  cycles.

The fatigue ductility coefficient,  $\epsilon_f'$ , and fatigue ductility exponent,  $c$ , are the intercept and slope of the best line fit to calculated true plastic strain amplitude ( $\Delta\epsilon_p/2$ ) versus reversals to failure ( $2N_f$ ) data in log-log scale:

$$\left( \frac{\Delta\epsilon_p}{2} \right)_{\text{calculated}} = \epsilon_f' (2N_f)^c \quad (11)$$

In accordance with ASTM Standard E739, when performing the least squares fit, the calculated true plastic strain amplitude ( $\Delta\epsilon_p/2$ ) was the independent variable and the reversals to failure ( $2N_f$ ) was the dependent variable. The calculated true plastic strain amplitude was determined from Equation 8. This plot is shown in Figure 10. To generate the  $\epsilon_f'$  and  $c$  values, the range of data used in this figure was chosen for  $[\Delta\epsilon_p/2]_{\text{calculated}} \geq 0.00020$  in/in and  $N_f \leq 10^5$  cycles.

The true strain amplitude versus reversals to failure plot is shown in Figure 11. This plot displays the strain - life curve (Eqn. 9), the elastic strain portion (Eqn. 10), the plastic strain portion (Eqn. 11), and superimposed fatigue data. A summary of the cyclic properties for SAE 4620 Quenched Core steel is provided in Table 2. Table A.2 in the Appendix provides the summary of the fatigue test results.

Table 1: Chemical composition of SAE 4620 Quenched Core steel

<b><u>Element</u></b>	<b><u>Wt. %</u></b>
Carbon, C	0.2%
Manganese, Mn	0.67%
Phosphorus, P	0.008%
Sulfur, S	0.030%
Silicon, Si	0.200%
Chromium, Cr	0.19%
Nickel, Ni	1.6%
Molybdenum, Mo	0.24%
Copper, Cu	0.16%
Tin, Sn	0.006%
Aluminum, Al	0.027%

## Table 2: Summary of the Mechanical Properties

<u>Microstructural Data</u>	<u>Average</u>			
<b>ASTM grain size number (MAG=500X):</b>				
The first longitudinal direction (L-T)	4 to 5			
<b>Inclusion rating number (MAG=100X):</b>				
Type A (sulfide type), thin series	2 1/2			
Type B (alumina type), thin series	None			
Type C (silicate type), thin series	None			
Type D (globular type), thin series	None			
<b>Hardness:</b>				
<b>Brinell (HB)</b>				
Transverse direction (T-T')	292.5			
The first longitudinal direction (L-T)	289.3			
<b>Rockwell B-scale (HRB)</b>				
Transverse direction (T-T')	105.2			
The first longitudinal direction (L-T)	105.0			
<b>Rockwell C-scale (HRC)</b>				
Transverse direction (T-T')	29.7			
The first longitudinal direction (L-T)	29.6			
<b>Microstructure type:</b>				
The first longitudinal direction (L-T)	ferrite/pearlite			
	<b>Average</b>		<b>Range</b>	
<b>Monotonic Properties</b>				
Modulus of elasticity, E, GPa (ksi):	210.7	(30,557.0)	209.9 - 211.5	(30,443.5 - 30,670.5)
Yield strength (0.2% offset), YS, MPa (ksi):	891.5	(129.3)	884.4 - 898.7	(128.3 - 130.3)
Upper yield strength UYS, MPa (ksi):	NA	NA		
Lower yield strength LYS, MPa (ksi):	NA	NA		
Yield point elongation, YPE (%)	NA			
Ultimate strength, S <sub>u</sub> , MPa (ksi):	963.7	(139.8)	961.5 - 965.9	(139.5 - 140.1)
Percent elongation, %EL (%)	43.0%		43.0% - 43.0%	
Percent reduction in area, %RA (%)	61.9%		61.2% - 62.7%	
Strength coefficient, K, MPa (ksi):	1,199.8	(174.0)	1,189.1 - 1,210.5	(172.5 - 175.6)
Strain hardening exponent, n:	0.0559		0.0537 - 0.0580	
True fracture strength, σ <sub>f</sub> *, MPa (ksi):	1651.9	(239.6)	1372.4 - 1931.4	(199.0 - 280.1)
True fracture ductility, ε <sub>f</sub> (%)	96.6%		94.6% - 98.6%	
	<b>Average</b>		<b>Range</b>	
<b>Cyclic Properties</b>				
Cyclic modulus of elasticity, E', GPa (ksi):	207.4	(30,078.4)	201.1 - 217.3	(29,163.1) - (31,515.0)
Fatigue strength coefficient, σ <sub>f</sub> ', MPa (ksi):	1,276.1	(185.1)		
Fatigue strength exponent, b:	-0.0713			
Fatigue ductility coefficient, ε <sub>f</sub> ' :	1.2368			
Fatigue ductility exponent, c:	-0.7051			
Cyclic yield strength, YS', MPa (ksi)	666.6	(96.7)		
Cyclic strength coefficient, K', MPa (ksi):	1,213.4	(176.0)		
Cyclic strain hardening exponent, n':	0.0964			

\* Correction was made according to the Bridgman correction factor.

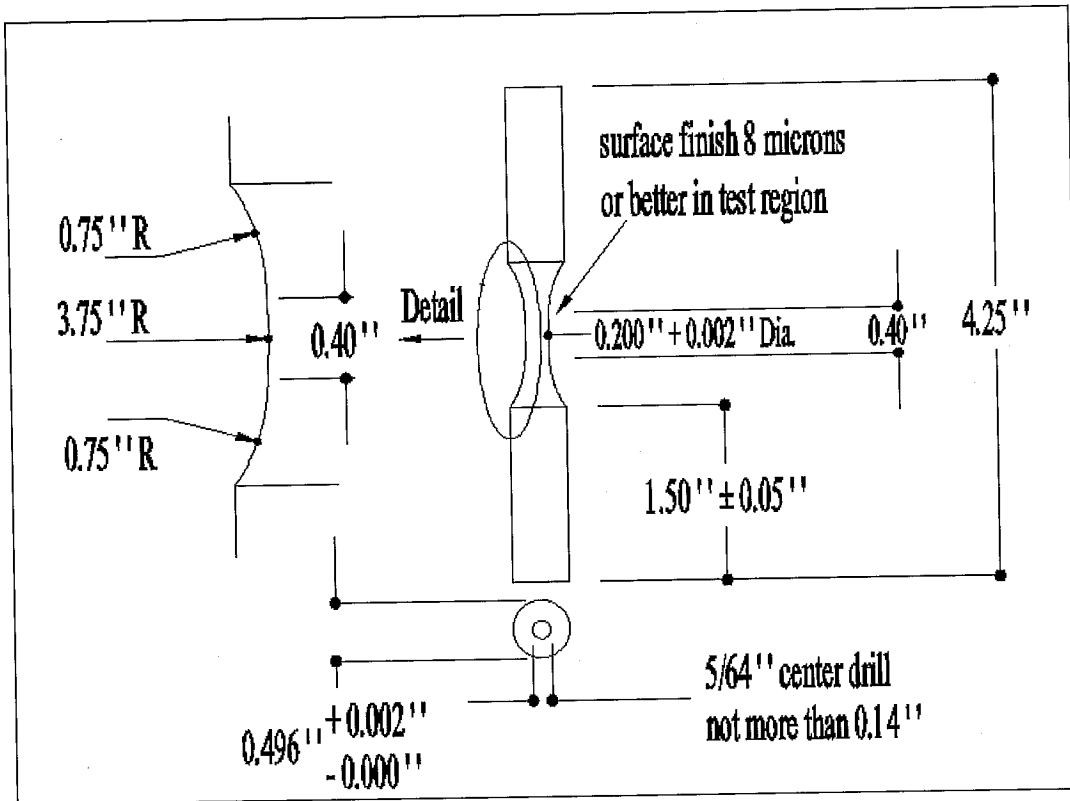


Figure 1: Specimen configuration and dimensions

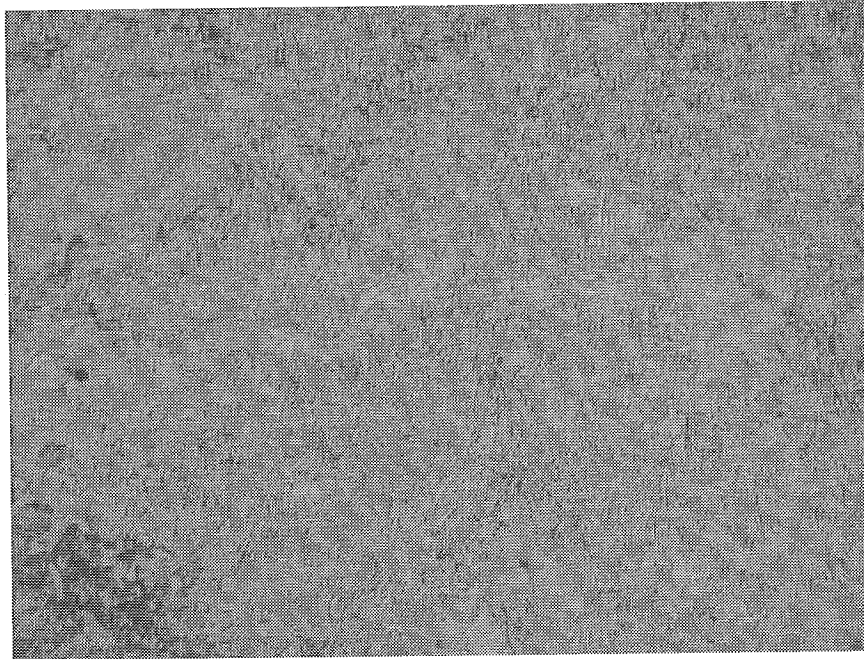
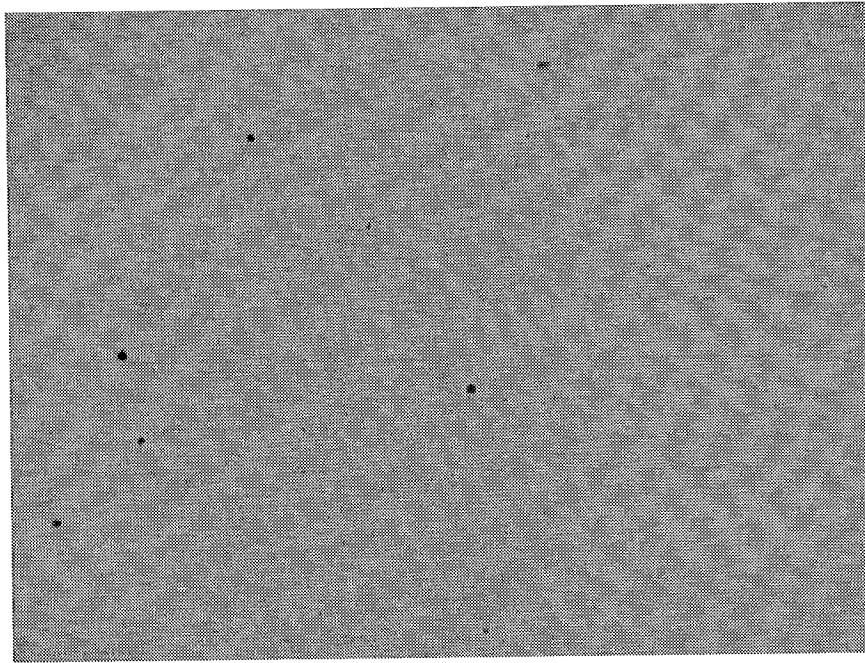


Figure 2: Photomicrograph in first longitudinal direction (L-T) at 500X for SAE 4620 Quenched Core steel (rolling direction is horizontal)



100  $\mu\text{m}$

Figure 3: Examples of inclusions in the first longitudinal direction (L-T) at 100X for SAE 4620 Quenched Core steel (rolling direction is horizontal)

**True Stress vs. True Plastic Strain**

E6-7  
 $\sigma = 1189.1(\epsilon_p)^{0.0537}$   
K = 1189.1MPa  
n = 0.0537  
R<sup>2</sup> = 0.9896

E6-6  
 $\sigma = 1210.5(\epsilon_p)^{0.058}$   
K = 1210.5MPa  
n = 0.058  
R<sup>2</sup> = 0.9899

Specimen ID:  
(top to bottom)  
E6-7  
E6-6

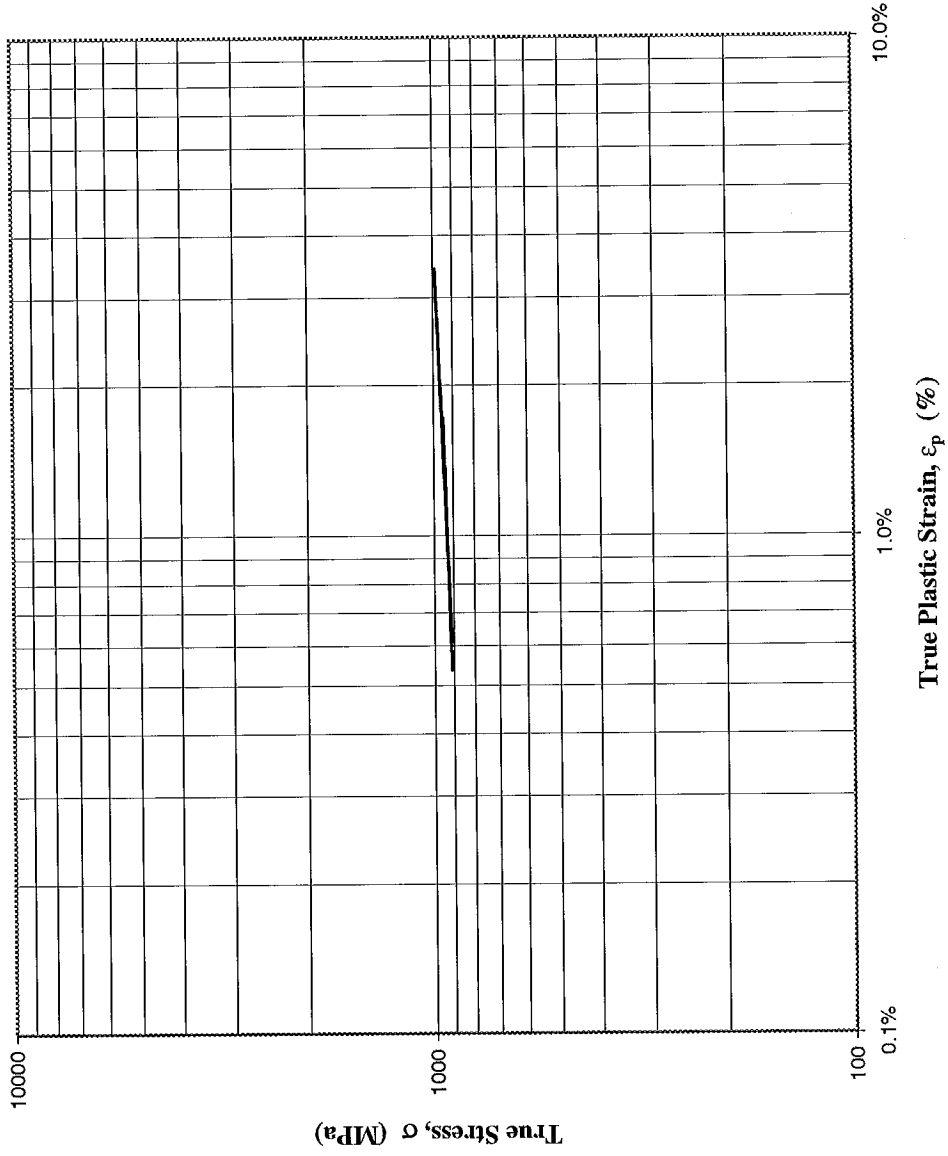


Figure 4: True stress versus true plastic strain

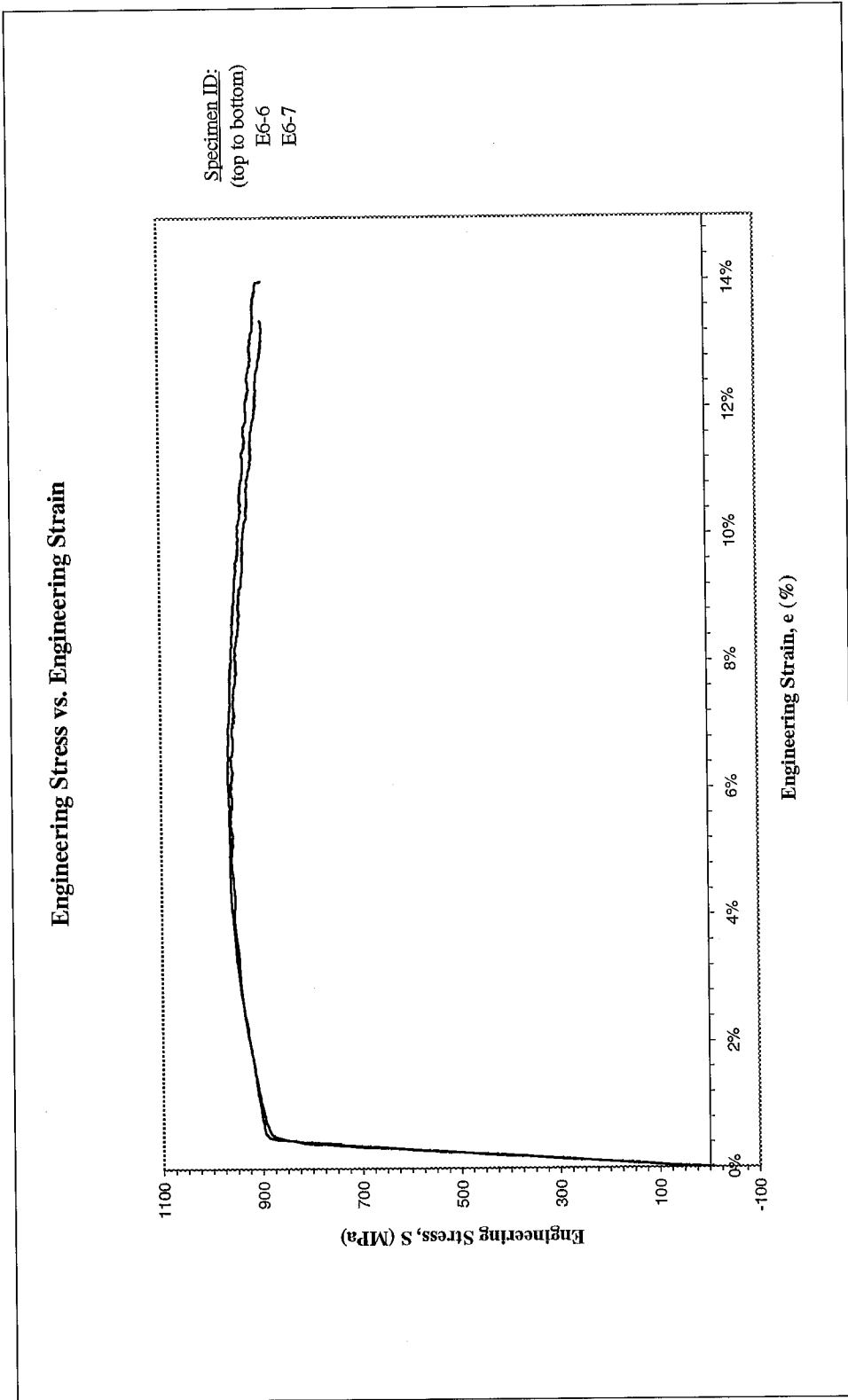


Figure 5: Monotonic stress-strain curve



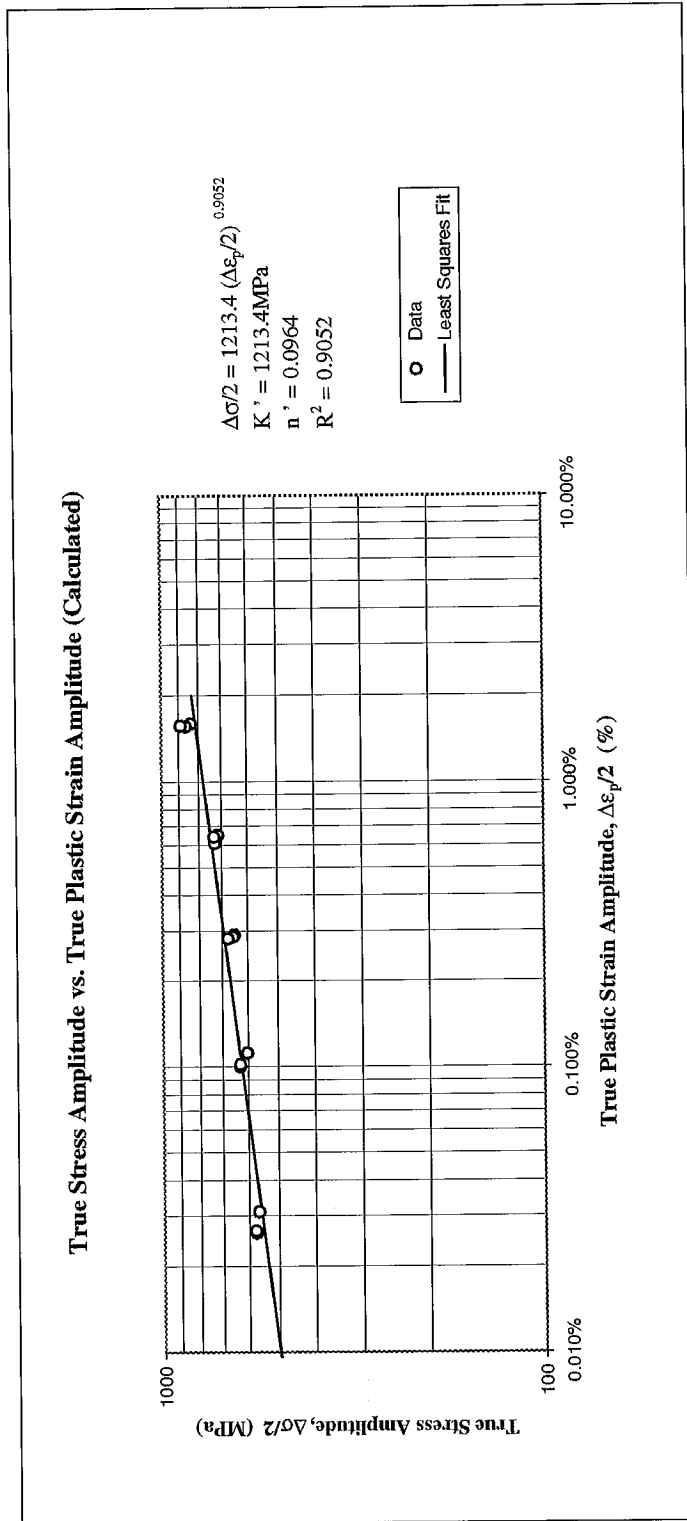


Figure 6: True stress amplitude versus calculated true plastic strain amplitude

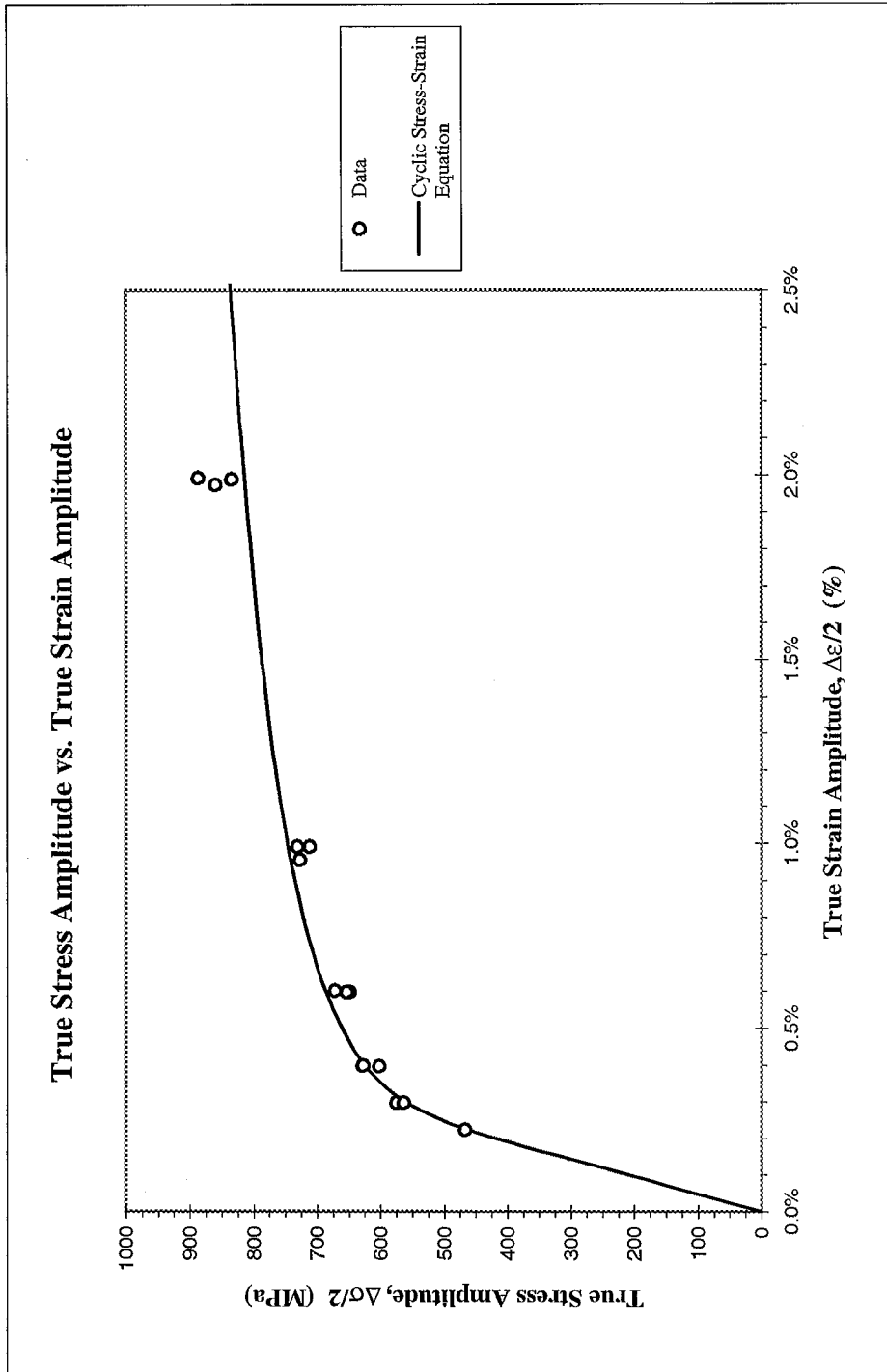


Figure 7: True stress amplitude versus true strain amplitude

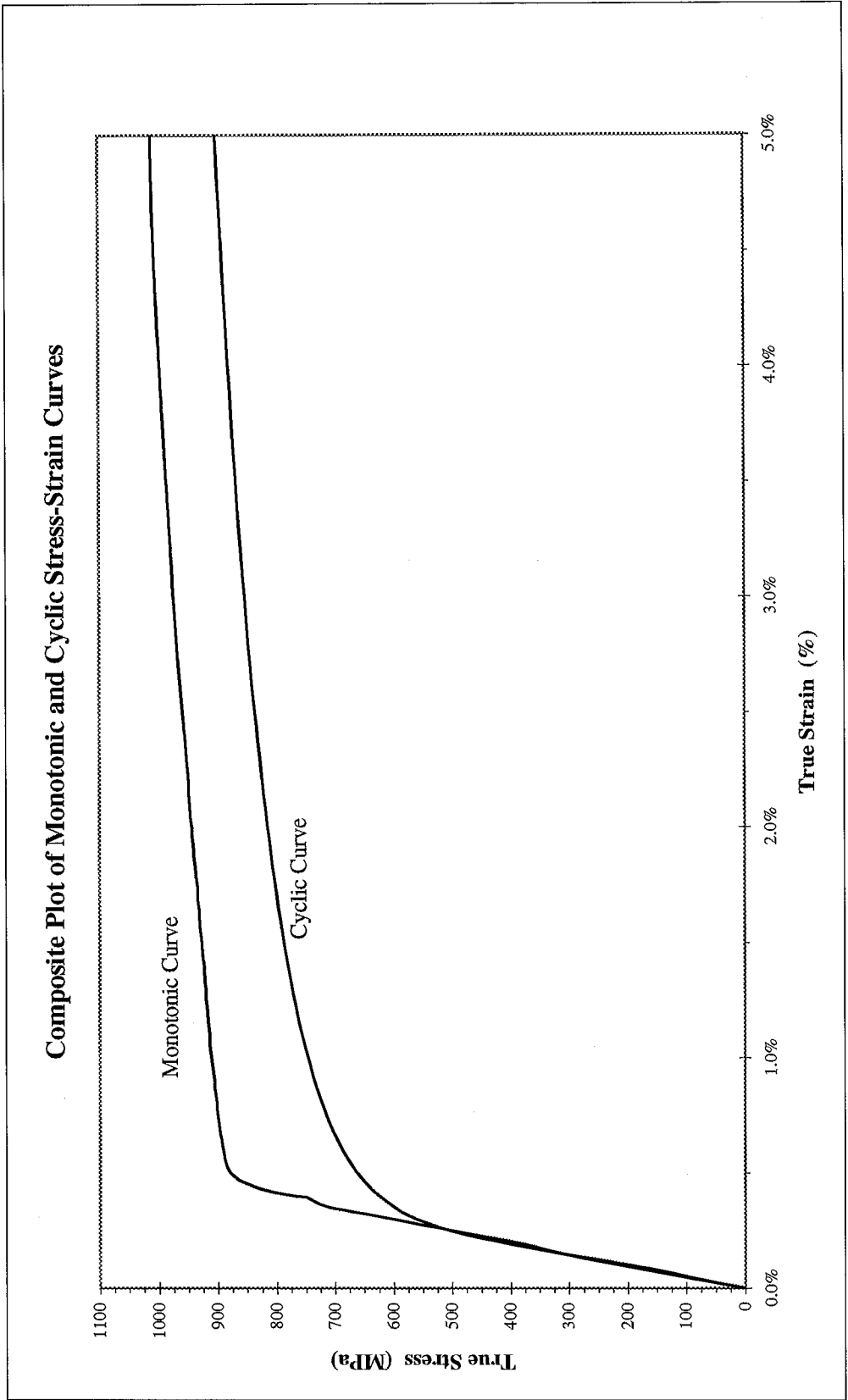


Figure 8: Composite plot of cyclic and monotonic stress-strain curves

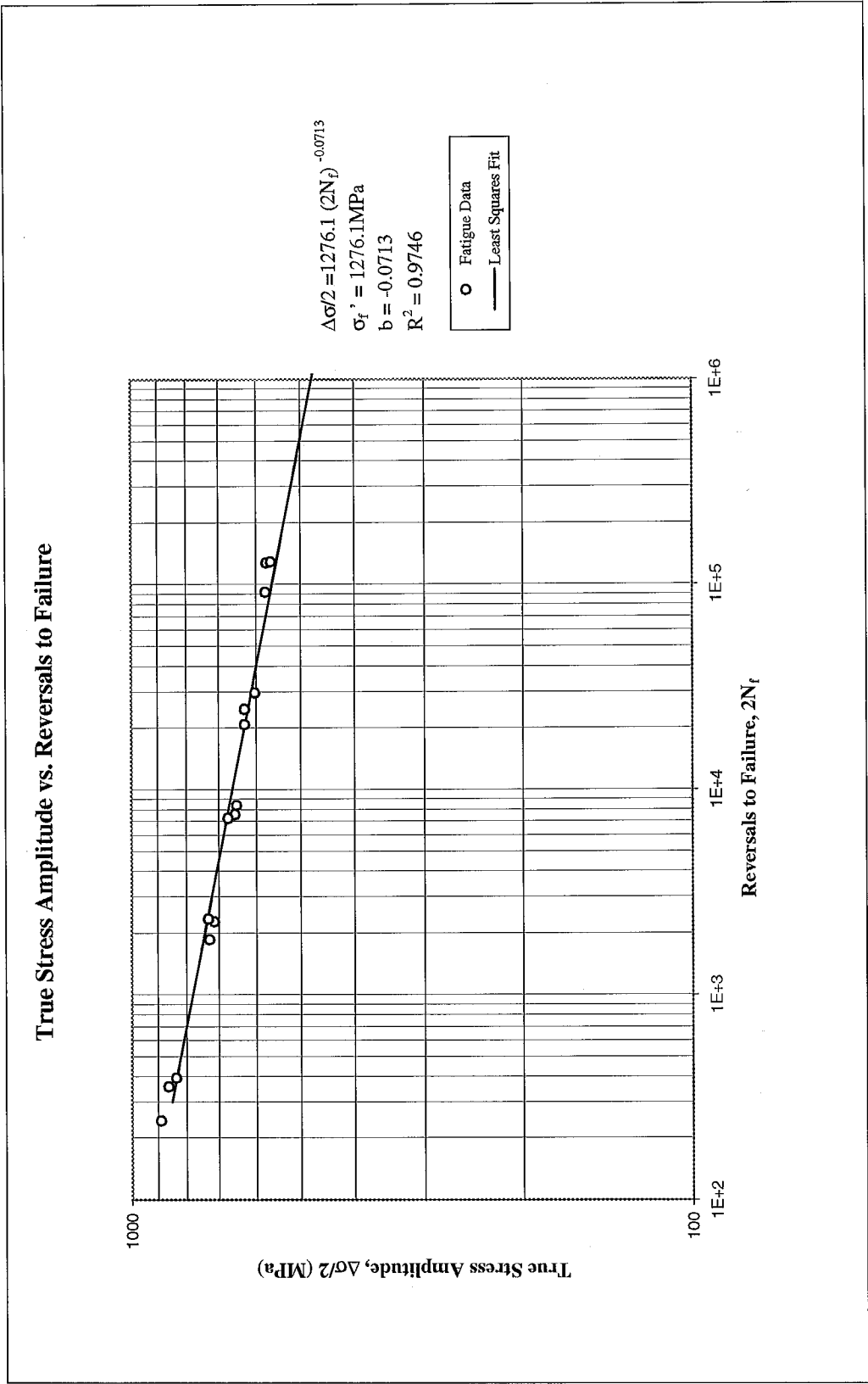


Figure 9: True stress amplitude versus reversals to failure

True Plastic Strain Amplitude (Calculated) vs. Reversals to Failure

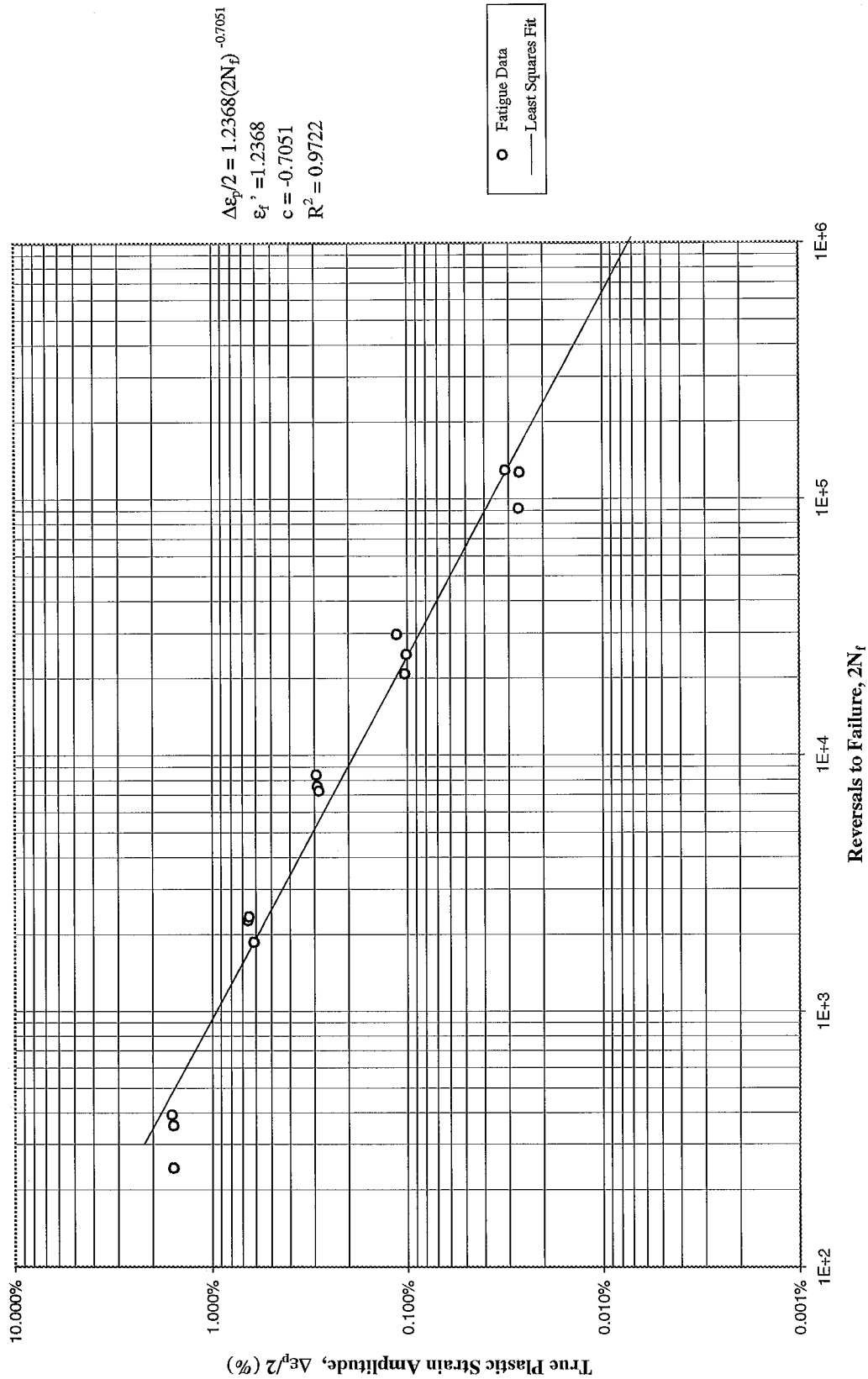


Figure 10: Calculated true plastic strain amplitude versus reversals to failure

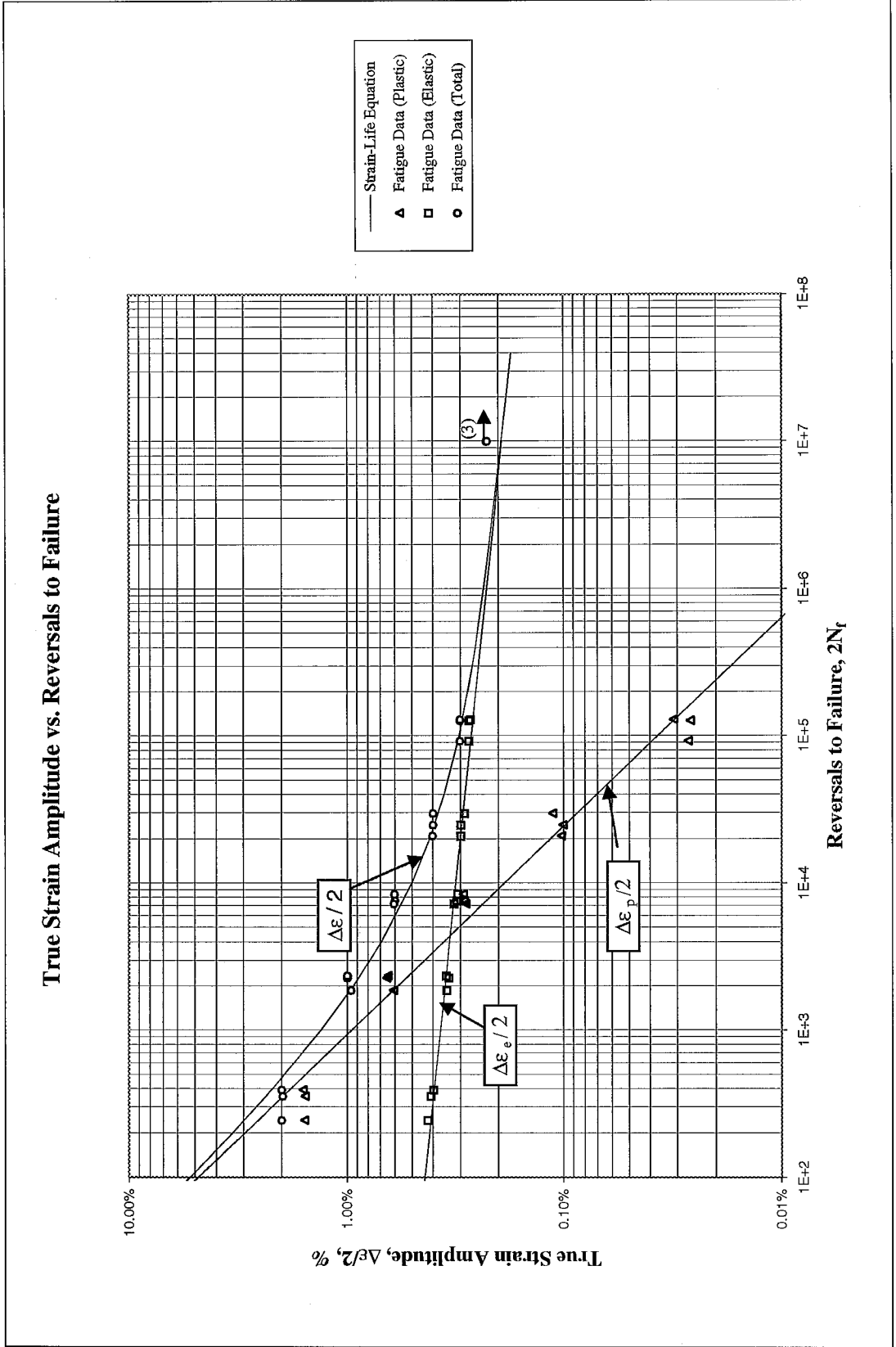


Figure 11: True strain amplitude versus reversals to failure

## REFERENCES

- [1] ASTM Standard E606-92, "Standard Practice for Strain-Controlled Fatigue Testing," Annual Book of ASTM Standards, Vol. 03.01, 1997, pp. 523-537.
- [2] ASTM Standard E83-96, "Standard Practice for Verification and Classification of Extensometers," Annual Book of ASTM Standards, Vol. 03.01, 1997, pp. 198-206.
- [3] ASTM Standard E1012-93a, "Standard Practice for Verification of Specimen Alignment Under Tensile Loading," Annual Book of ASTM Standards, Vol. 03.01, 1997, pp. 699-706.
- [4] ASTM Standard E8-96a, "Standard Test Methods for Tension Testing of Metallic Materials," Annual Book of ASTM Standards, Vol. 03.01, 1997, pp. 56-76.
- [5] ASTM Standard E112-96, "Standard Test Methods for Determining Average Grain Size," Annual Book of ASTM Standards, Vol. 03.01, 1997, pp. 227-249.
- [6] ASTM Standard E45-97, "Standard Test Methods for Determining the Inclusion Content of Steel," Annual Book of ASTM Standards, Vol. 03.01, 1997, pp. 157-170.
- [7] ASTM Standard E739-91, "Standard Practice for Statistical Analysis of Linear or Linearized Stress-Life (S-N) and Strain-Life ( $\epsilon$ -N) Fatigue Data," Annual Book of ASTM Standards, Vol. 03.01, 1995, pp. 615-621.
- [8] ASTM Standard E646-93, "Standard Test Method for Tensile Strain-Hardening Exponents (n-values) of Metallic Sheet Materials," Annual Book of ASTM Standards, Vol. 03.01, 1997, pp. 550-556.
- [9] Bridgman, P. W., "Stress Distribution at the Neck of Tension Specimen," *Transactions of American Society for Metals*, Vol. 32, 1944, pp. 553-572.

# APPENDIX



**Table A.1: Summary of monotonic tensile test results**

Specimen ID	D <sub>o</sub> , mm (in.)	D <sub>f</sub> , mm (in.)	L <sub>o</sub> , mm (in.)	L <sub>f</sub> , mm (in.)	E, GPa (ksi)	YS (offset=0.2%), MPa (ksi)	UYS, MPa (ksi)	LYS, MPa (ksi)	YPE, %	S <sub>u</sub> , MPa (ksi)	K, MPa (ksi)	n	%EL, %	%RA, %	R, mm (in.)	σ <sub>f</sub> *, MPa (ksi)	ε <sub>f</sub>
E6-6	5.23 (0.206)	3.20 (0.126)	7.62 (0.30)	10.90 (0.43)	211.5 (30,670.5)	884.4 (128.3)	NA NA	NA NA	NA	965.9 (140.1)	1,210.5 (175.6)	0.058	43%	63%	1.64 (0.065)	1372.4 (199.0)	99%
E6-7	5.18 (0.204)	3.23 (0.127)	7.62 (0.30)	10.89 (0.43)	209.9 (30,443.5)	898.7 (130.3)	NA NA	NA NA	NA	961.5 (139.5)	1,189.1 (172.5)	0.0537	43%	61%	1.72 (0.068)	1931.4 (280.1)	95%
Average values					210.7 (30,557.0)	891.5 (129.3)	NA NA	NA NA	NA	963.7 (139.8)	1199.8 (174.0)	0.0559	43%	62%	1.68 0.066	1651.9 (239.6)	97%

\* The values of true fracture strength are corrected for necking according to the Bridgman correction factor.

**Table A.2: Summary of constant amplitude completely reversed fatigue test results**

Specimen ID	Test control mode	Test freq., Hz	E, GPa (ksi)	At midlife ( $N_{50\%}$ )						$2N_{50\%}$ , <sup>[a]</sup> reversals	$(2N_f)_{50\%}$ , <sup>[b]</sup> reversals	Failure location <sup>[c]</sup>
				E', GPa (ksi)	$\Delta\epsilon/2$ , %	$\Delta\epsilon_p/2$ (calculated), %	$\Delta\epsilon_p/2$ (measured), %	$\Delta\sigma/2$ , MPa (ksi)	$\sigma_m$ , MPa (ksi)			
E6-3	strain	0.20	209.6 (30,401.7)	203.5 (29,519.4)	1.990%	1.594%	1.584%	834.2 (121.0)	-9.5 (-1.4)	200	394	IGL
E6-21	strain	0.20	204.1 (29,595.5)	210.4 (30,507.8)	1.974%	1.566%	1.550%	859.9 (124.7)	-11.5 (-1.7)	200	358	IGL
E6-20	strain	0.20	206.8 (29,989.6)	205.4 (29,788.9)	1.994%	1.573%	1.582%	886.7 (128.6)	6.7 (1.0)	130	244	IGL
E6-1	strain	0.50	215.0 (31,181.2)	212.0 (30,743.3)	0.957%	0.612%	0.595%	727.0 (105.4)	-4.5 (-0.7)	924	1,874	IGL
E6-26	strain	0.50	209.3 (30,360.7)	202.0 (29,292.9)	0.992%	0.654%	0.633%	711.8 (103.2)	-3.8 (-0.5)	1,000	2,280	IGL
E6-14	strain	0.50	208.6 (30,255.6)	205.9 (29,861.9)	0.991%	0.644%	0.635%	730.7 (106.0)	-5.8 (-0.8)	1,000	2,356	IGL
E6-2	strain	0.83	209.6 (30,393.2)	207.6 (30,102.6)	0.600%	0.292%	0.272%	648.6 (94.1)	-1.4 (-0.2)	4,000	8,428	IGL
E6-25	strain	0.83	206.2 (29,902.2)	205.6 (29,818.7)	0.598%	0.288%	0.275%	653.6 (94.8)	-2.1 (-0.3)	4,000	7,604	IGL
E6-16	strain	0.83	208.8 (30,290.0)	202.0 (29,301.0)	0.602%	0.283%	0.270%	672.3 (97.5)	-4.8 (-0.7)	4,000	7,270	IGL
E6-4	strain	2.5	203.8 (29,563.0)	210.0 (30,452.7)	0.399%	0.101%	0.107%	628.2 (91.1)	0.1 (0.0)	10,000	24,888	IGL
E6-18	strain	2.5	203.3 (29,486.7)	207.4 (30,086.2)	0.398%	0.112%	0.110%	601.9 (87.3)	26.0 (3.8)	10,000	29,828	IGL
E6-15	strain	2.5	207.0 (30,025.1)	211.2 (30,633.1)	0.400%	0.102%	0.105%	627.5 (91.0)	0.2 (0.0)	10,000	20,892	IGL
E6-5	strain	3.0	210.9 (30,590.0)	217.3 (31,515.0)	0.299%	0.027%	0.032%	573.0 (83.1)	19.9 (2.9)	40,000	127,746	IGL
E6-8	strain	3.0	209.4 (30,375.1)	201.1 (29,163.1)	0.299%	0.026%	0.037%	575.4 (83.5)	29.6 (4.3)	50,000	92,200	IGL
E6-19	strain	3.0	209.0 (30,311.8)	208.6 (30,258.9)	0.298%	0.031%	0.039%	563.3 (81.7)	85.2 (12.4)	50,220	129,972	IGL
E6-24	strain	3.0	203.2 (29,467.2)	208.3 (30,208.2)	0.225%	0.004%	0.002%	467.0 (67.7)	301.4 (43.7)	159,536	10,000,000	None
	load	30					467.0 (67.7)	0.0 (0.0)				
E6-23	load	30					466.5 (67.7)	0.0 (0.0)			10,000,000	None
E6-22	load	30					466.3 (67.6)	0.0 (0.0)			10,000,000	None

[a]  $N_{50\%}$  is defined as the midlife cycle (for run-out tests, data is taken from the stable cycle indicated).

[b]  $(N_f)_{50\%}$  is defined as 50% load drop.

[c] IGL = inside gage length; AKP = at knife point; OGIT = outside gage length but inside test section.

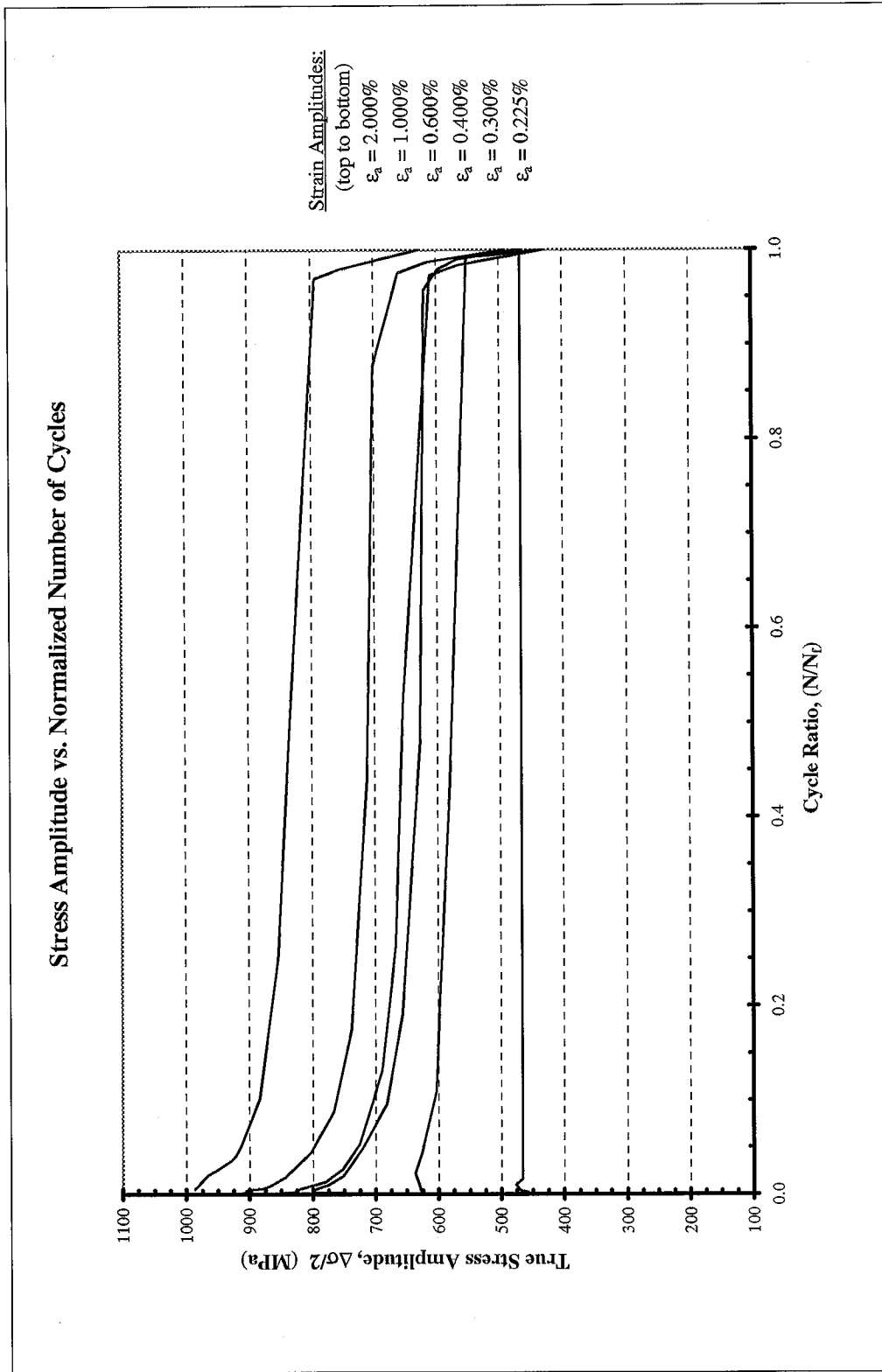


Figure A.1a: True stress amplitude versus normalized number of cycles

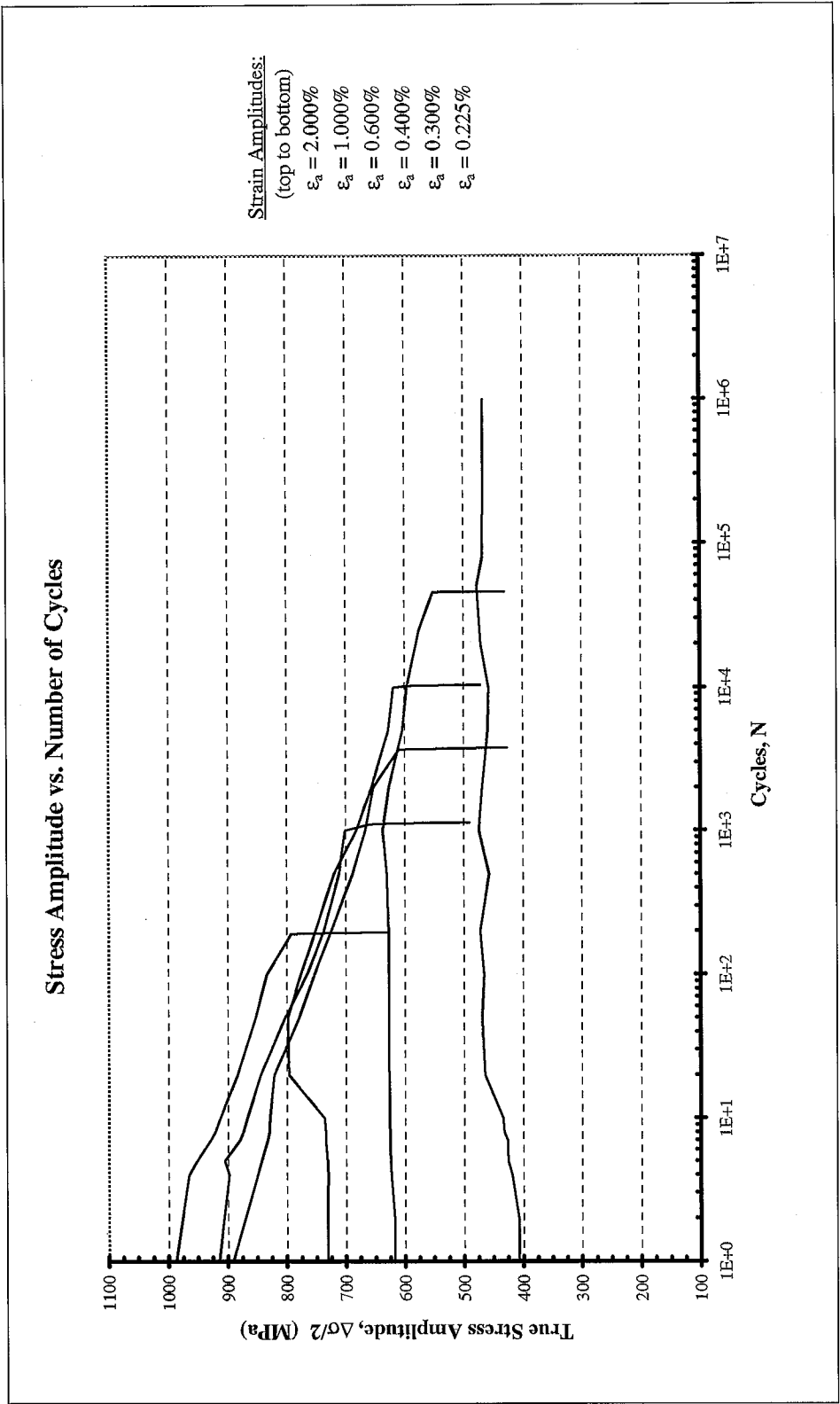


Figure A.1b: True stress amplitude versus number of cycles

### Composite Plot of Midlife Hysteresis Loops

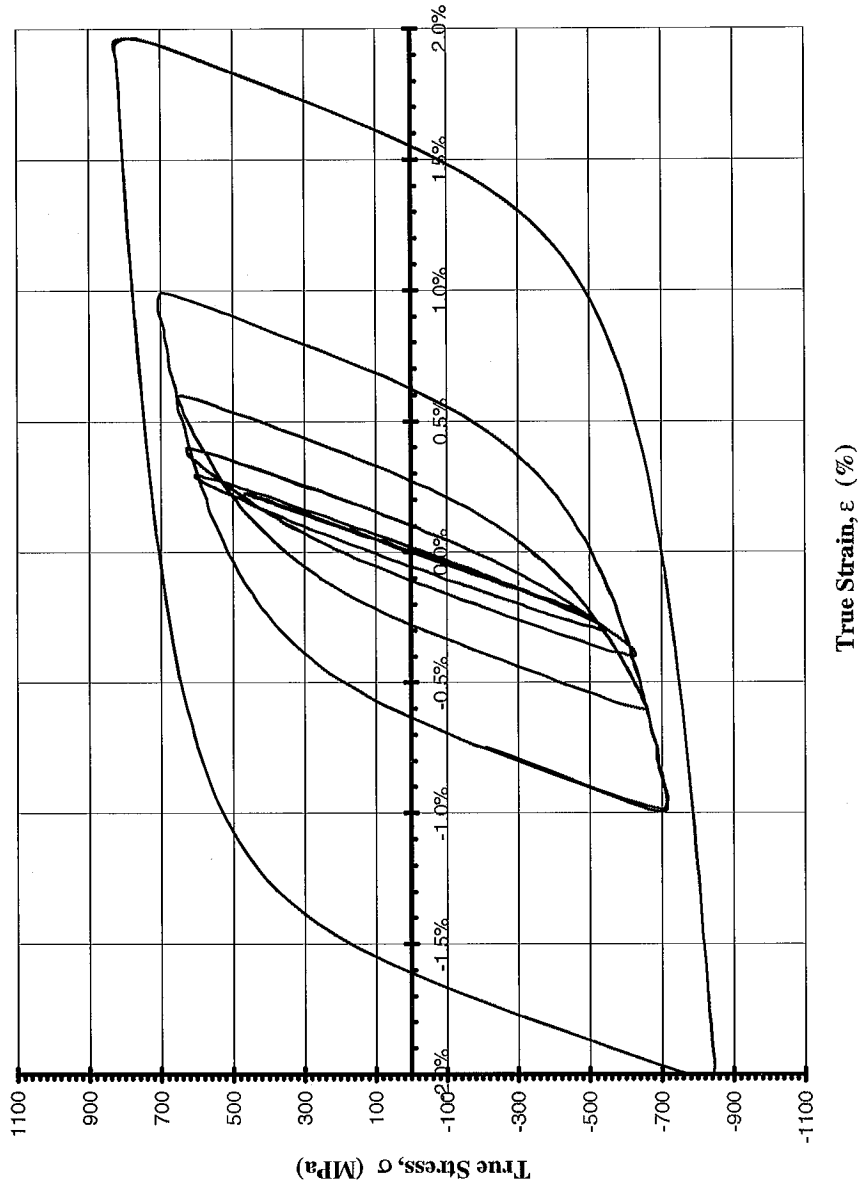


Figure A.2: Composite plot of midlife hysteresis loops